Microelectronics Reliability 178 (2026) 116013

Contents lists available at ScienceDirect

Microelectronics Reliability

journal homepage: www.elsevier.com/locate/microrel

Research paper

Predictive modeling for aging performance of quantum dots composite under temperature-humidity dual stress coupling effect

Xuan Yang [a], Linyi Xiang [a], Bin Xie [b,*], Xiaobing Luo [a,*]

[a] School of Energy and Power Engineering, Huazhong University of Science and Technology, Wuhan, 430074, China
[b] School of Mechanical Science and Engineering, Huazhong University of Science and Technology, Wuhan, 430074, China

ARTICLE INFO

Keywords:
Quantum dots
Predictive model
Temperature-humidity dual stress
Reliability

ABSTRACT

Quantum dots (QDs) face significant challenges in high-temperature and high-humidity environments, where both thermal and humidity-induced degradation as well as humidity-induced enhancement can occur simultaneously. This dual stress coupling effect can lead to complex intensity evolution in QDs. Given the critical importance of performance and lifetime prediction in optoelectronic devices, a systematic study and predictive modeling of the aging performance of QDs under temperature-humidity conditions are essential. In this work, we experimentally investigated the light intensity evolution of QDs composites under various temperature-humidity conditions. The results showed both increases and decreases in intensity within a single aging curve. By analyzing the underlying mechanisms of these intensity changes, we developed a predictive model by modifying the Kohlrausch-Williams-Watts equation with an asymmetric Gaussian pulse function (AsG-KWW), which demonstrated excellent agreement with the experimental data under each aging condition. According to this model, three distinct stages were identified: a sharp initial intensity drop, a recovery, and a stable attenuation. Additionally, the mean time to failure (MTTF) of the samples was derived and analyzed using the AsG-KWW model. Analysis of the fitting parameters revealed that intensity recovery only occurred under relatively mild aging conditions.

1. Introduction

Quantum dots (QDs) have emerged as widely utilized nanocrystals in optoelectronic applications in recent years [1–3]. This primarily due to their remarkable properties such as high color purity, wide absorption spectra, and tunable emission spectra [4,5]. However, their optical performance is highly susceptible to degradation under high-temperature and high-humidity operating conditions. These environmental stresses can induce structural changes in QDs, compromising their performance and stability [6]. Under thermal stress, trap states are formed due to thermally induced ligand detachment and lattice mismatch between the core and shell materials [7]. In humid environments, water and oxygen molecules can also promote trap states formation through ligand detachment and oxidation of the core/shell structure [8]. These trap states facilitate non-radiative relaxation process, leading to a decline in photoluminescence intensity [9]. Conversely, water and oxygen molecules can also passivate the trap states on QDs, repopulating electrons from the trap states to conduction band. This process enhances band-edge radiative recombination and can lead to temporary increase in light intensity [10]. While improving quantum efficiency and thermal management are key industry approaches for enhancing QDs reliability [11–13], they still face severe degradation under high-temperature and high-humidity conditions, which motivates the present predictive modeling study.

Numerous studies have been conducted to investigate the aging behavior of QDs under and humidity stresses [14–16]. In our previous work, QDs-silicone were aged by immersion in deionized water [17]. The light intensity exhibited a sharp decline of 60% within the first 48 h, and further decreased to 24% of its initial value at 360 h. In contrast, light intensity enhancement was observed in QDs-glass, where the intensity increased by 11% during the first 96 h, then declined by 5%. Pei et al. investigated the light intensity evolution of QDs/silicone under 50 °C and 99.8% relative humidity (RH), reporting a reduction of 46% of the initial intensity after 168 h [18]. Xie et al. tested the red-light intensity of QDs-LEDs at 85 °C and 85% RH for 168 h, observing an exponential decay trend [19]. However, existing studies on QDs' performance under combined temperature and humidity conditions have not systematically studied the coupling effect of these two factors. More

* Corresponding authors.
E-mail addresses: binxie@hust.edu.cn (B. Xie), luoxb@hust.edu.cn (X. Luo).

https://doi.org/10.1016/j.microrel.2026.116013
Received 3 August 2025; Received in revised form 29 December 2025; Accepted 16 January 2026

importantly, a robust predictive model capable of capturing both the rise and fall of light intensity during aging is urgently needed for rapid evaluation of QDs' stability and lifetime.

In this work, we experimentally investigated the light intensity evolution of QDs composites under various temperature-humidity conditions. Base on the experimental results, we developed a predictive model by modifying the Kohlrausch-Williams-Watts (KWW) equation with an asymmetric Gaussian pulse function, referred to as AsG-KWW. This model effectively captured the underlying mechanisms governing the rise and fall of light intensity in QDs composites and exhibited excellent agreement with experimental aging curves under all tested conditions. Using the AsG-KWW model, we identified three characteristic stages in the aging process, each associated with distinct mechanisms: 1) sharp initial drop; 2) recovery; 3) stable attenuation. Furthermore, the mean time to failure (MTTF) of QDs composites was derived from the model, and relevant fitting parameters were analyzed. Notably, the recovery stage was observed only under relatively mild aging conditions.

2. Method

2.1. Asymmetric Gaussian pulse function modified Kohlrausch-Williams-Watts model

Kohlrausch-Williams-Watts (KWW) function is used to describe baseline attenuation behavior of QDs' light intensity under the coupling effect of temperature-humidity dual stress with two adjustable parameters [20]:

$$I_{\text{base}}(t) = e^{-\left(\frac{t}{\tau}\right)^{\beta}} \tag{1}$$

where β is dimensionless stretched exponent, and τ is characteristic lifetime. Asymmetric Gaussian (AsG) pulse function is employed as a modifying term to identify the abnormal recovery stage [21]:

$$\text{AsG}(t) = \begin{cases} Ce^{-0.5\left(\frac{t-t_0}{\sigma_1}\right)^{\alpha}}, t < t_0 \\ Ce^{-0.5\left(\frac{t-t_0}{\sigma_2}\right)^{\alpha}}, t > t_0 \end{cases} \tag{2}$$

where C is Gaussian pulse exponent which represents the extent of the increase in intensity, t_0 is central time of the abnormal recovery stage, σ_1 and σ_2 are the pulse widths. α is the shape factor of the function relating to the varying rate of intensity of the abnormal recovery stage. The Asymmetric Gaussian pulse function modified Kohlrausch-Williams-Watts (AsG-KWW) model $I_{\text{AsG}}(t)$ are obtained by combining Eqs. (1) and (2):

$$I_{\text{AsG}}(t) = I_{base}(t) \times (1 + \text{AsG}(t)) = \begin{cases} e^{-\left(\frac{t}{\tau}\right)^{\beta}} \times \left(1 + Ce^{-0.5\left(\frac{t-t_0}{\sigma_1}\right)^{\alpha}}\right), t < t_0 \\ e^{-\left(\frac{t}{\tau}\right)^{\beta}} \times \left(1 + Ce^{-0.5\left(\frac{t-t_0}{\sigma_2}\right)^{\alpha}}\right), t > t_0 \end{cases}, \quad 0 < \beta, C \le 1, \quad \alpha = 0, 2, 4... \tag{3}$$

Genetic Algorithm (GA) was adopted to fit the experimental curves by finding the optimal parameters in the equations. The fitness function was defined by the mean error (ME) between predictive model and experimental data:

$$\text{Fitness} = \sum_{1}^{n} |I_{\text{AsG}} - I_{\text{Exp}}| \Big/ n \tag{4}$$

where n is the number of the experimental data. The parameters for GA optimization are shown in Table I. p_1 and p_2 are the mutation and crossover probabilities, respectively.

2.2. Weibull distribution

Weibull distribution was utilized to determine the mean time to failure (MTTF). The unreliability of QDs composites $F(t)$ is [22]:

$$F(t) = 1 - e^{\left[-\left(\frac{t}{\eta}\right)^{m}\right]} \tag{5}$$

where m is the shape factor of the device, η is the scale factor. MTTF equals η when device unreliability is 0.368. Take the logarithm twice on both sides of Eq. (5):

$$\ln\ln[1 - F(t)]^{-1} = m\ln t - m\ln\eta \tag{6}$$

set a function:

$$y(x) = ax + b \tag{7}$$

and

$$y = \ln\ln[1 - F(t)]^{-1}, x = \ln t, a = m, b = -m\ln\eta \tag{8}$$

If $\ln t$ and $\ln\ln[1\text{-}F(t)]^{-1}$ is well fitted by Eq. (7), it is considered that the samples' lifetime follows the Weibull distribution. The unreliability $F(t)$ in the ordinate can be calculated using the median rank formula [23]:

$$F(t_j) = \frac{j - 0.3}{n + 0.4}, j = 1, 2, 3, ..., n \tag{9}$$

where j is the number of the failed samples at t_j, and n is the number of the tested samples. After obtaining parameters a and b through fitting, the MTTF can be calculated as follow:

$$\text{MTTF} = \eta = e^{-a/b} \tag{10}$$

2.3. Experimental validations

Red-emissive CdSe/ZnS QDs with a peak wavelength of 630 nm were provided by Poly Opto-Electronics (China). Two component silicone was purchased from Dowsil (SYLGARD 184, A:B = 10:1). 60 μl QDs-toluene solution (10 mg/ml) was uniformly mixed with 2 g silicone gel and then degassed. Subsequently, the mixture was poured into an aluminum alloy mold (with a diameter of 12.7 mm and thickness of 1.5 mm) and cured at 85 °C for 15 min. The photoluminescence (PL) spectrum was tested by a Fluorescence spectrofluorometer (EI FLS980, Edinburgh Instruments) at a pulse excitation wavelength of 450 nm. Six parallel samples were adopted for aging test. The aging conditions were built by a humidity chamber (BTH-150, GDBELL). The samples were excited by a blue light-emitting LED with a peak wavelength of 450 nm and a driving current of 100 mA (SkyBright). The light intensity was obtained by an integrating sphere system (ATA-1000, Everfine). Fig. 1 illustrates the light output profile in 160 days. The value only varied by 3.6%, which is completely acceptable.

Table I
GA optimization parameters.

Population size	Tolerance	p_1	p_2	Maximum iterations
500	1.0×10^{-4}	0.01	0.6	500

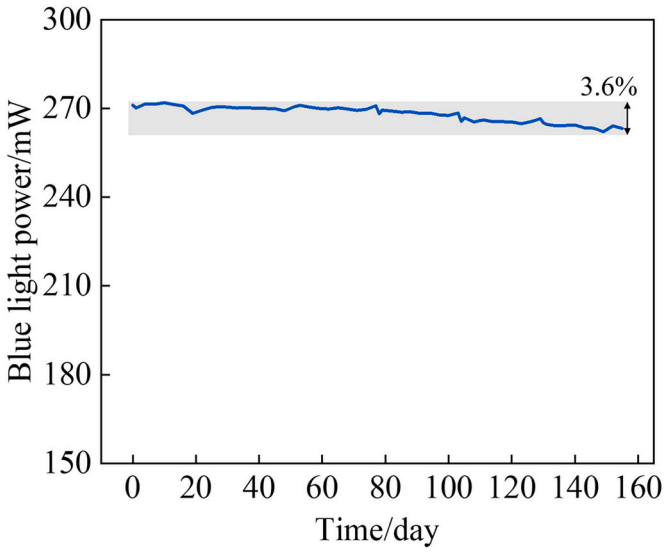

Fig. 1. Light output profile of the light source.

3. Results and discussion

The QDs composite samples were subjected to six different aging conditions [T40H80 (40 °C, 80% RH), T60H60 (60 °C, 60% RH), T60H70 (60 °C, 70% RH), T60H80 (60 °C, 80% RH), T60H90 (60 °C, 90% RH), and T80H80 (80 °C, 80% RH)], for a duration of 600 h. Under these aging conditions, the intensity degradation rate is moderate. Thereby we can collect enough detailed information to study the aging behavior of QDs composites. If the temperature is too high (>80 °C), the intensity recovery is too short to observe, and if the humidity is too low (<50% RH), the intensity recovery is too small to observe. Fig. 2a and b show the photographs of six QDs composites under daylight and UV light, respectively. Fig. 2 displays a narrow photoluminescence (PL) spectrum of. QDs composites with a peak wavelength of 630 nm. Fig. 3 shows the time-resolved light intensity curves under these conditions. Across all conditions, the aging behavior exhibited a nonconventional degradation pattern characterized by an initial sharp intensity drop followed by a temporary recovery stage in most cases, and ended with a stable attenuation stage in some cases. Specifically, all samples showed a pronounced sharp drop in intensity within the first 24 h, which is attributed to structural destruction due to dramatically improved thermal stress and the sudden infiltration of water and oxygen molecules. Among them, under T40H80 condition, it showed the smallest initial drop of ~15%, while the T80H80 condition exhibited the most severe, approximately 40%, with no evident recovery afterward. In contrast, a strong recovery stage was observed under T60H70, where the intensity rebounded by nearly 30% after the initial decline. For most conditions, the recovery stage was temporary, and it followed by an eventual stable attenuation in T60H80 and T60H90. The recovery stage was defined as the period starting from intensity rise and ending when the intensity drops back to the initial value at the onset of recovery, encompassing both the rise and subsequent fall. The recovery stage appeared in all conditions except T80H80. Within the recovery stage, both rise and fall in intensity occurred, governed by following competing mechanisms: when humidity-induced enhancement outweighed thermally and humidity-induced degradation, intensity increased; otherwise, it declined. This recovery effect was temporary. Eventually, all curves entered a final stage of stable exponential decay, observed prominently under T60H80, T60H90, and T80H80.

The extent and dynamics of the intensity changes were found to be strongly dependent on the aging temperature and humidity. At a fixed temperature of 60 °C (Fig. 3b–e), higher humidity levels led to more rapid degradation, shorter recovery durations, and earlier onset of the transition from rise to fall in recovery stage. For example, under T60H90, the transition occurred at 168 h, which is earlier than the 240-h mark under T60H80. Meanwhile, the remaining normalized intensity values after 600 h were approximately 0.8 for T60H60, 0.85 for T60H70, 0.5 for T60H80, and 0.7 for T60H90. When humidity was held constant at 80% RH (Fig. 3a, d, and f), temperature had a pronounced influence. The initial sharp drop was improved as increasing temperature as about 15% for T40H80, 20% for T60H80, and 40% for T80H80. Meanwhile, the remaining normalized intensity value were about 0.9 for T40H80, 0.5 for T60H80, and 0.4 for T80H80. The recovery duration significantly decreased with increasing temperature, from T40H80 to T80H80. T40H80 exhibited a long-lasting recovery stage with no observable secondary drop during the test, while T80H80 showed no recovery phase at all. In summary, both temperature and humidity play critical, coupled roles in the degradation dynamics of QDs composites. Extra energy provided by the high temperature may accelerate the chemical reaction between water/oxygen molecules and QDs. Higher temperature and humidity levels exacerbate structural damage, promote trap-state formation, and diminish the duration and amplitude of recovery, ultimately leading to a faster and more pronounced attenuation of light intensity.

KWW equation is widely used to describe the relaxation process in materials subjected to complex environmental conditions. Fig. 4a presents the KWW curves featuring different parameters. In this model, τ represents the characteristic lifetime, defined as the time at which the relative light intensity decreases to 36.8% of its initial value. The parameter β is a dimensionless exponent that characterizes the variation

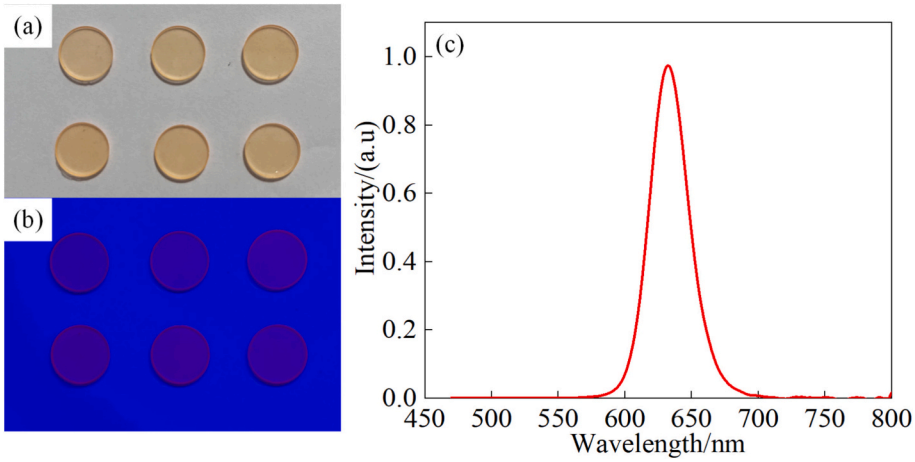

Fig. 2. Photographs of tested QDs composites. (a) Under daylight; (b) Under UV light; (c) PL spectrum.

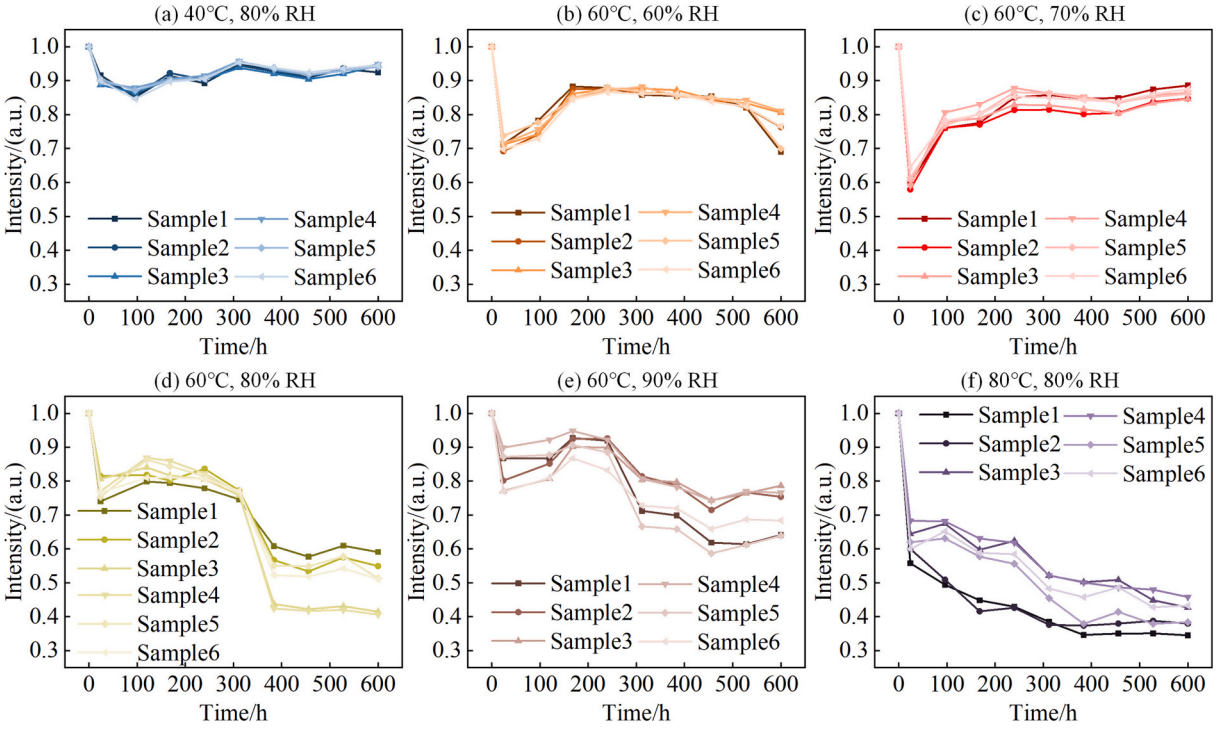

Fig. 3. Normalized time-evolved intensity curves of QDs composites. (a) 40 °C, 80% RH, (b) 60 °C, 60% RH, (c) 60 °C, 70% RH, (d) 60 °C, 80% RH, (e) 60 °C, 90% RH, and (f) 80 °C, 80% RH.

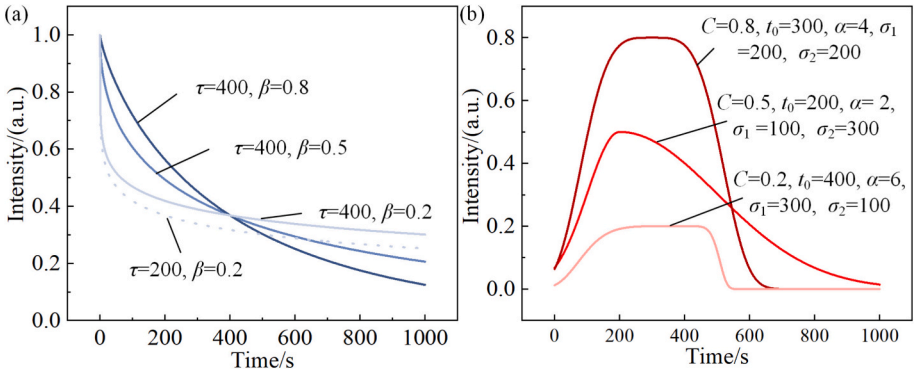

Fig. 4. Curves with different parameters. (a) KWW equation; (b) AsG pulse function.

in the slope of the curve: a smaller β indicates a steeper decline in the early aging stage and a gentler slop in the later stage. To describe the recovery behavior observed in QDs composites, an AsG pulse function was introduced. Fig. 4b illustrates the AsG pulse function under various parameter settings. It was chosen for the temporary and asymmetric perfectly aligned with the increase and decrease trend in the recovery process. In this function, σ_1 and σ_2 denote the durations of the rise and fall processes within recovery stage, respectively, a larger α corresponds to a flatter peak indicating a smaller intensity varying rate. The KWW equation was employed to represent the baseline attenuation due to thermal and humidity-induced degradation, while the AsG pulse function accounts for the short-term, asymmetric recovery behavior attributed to humidity-induced enhancement. The AsG component serves as a corrective term superimposed on the KWW baseline. Specifically, the KWW function captures the long-term, irreversible degradation effects driven by temperature and humidity, whereas the AsG function models the temporary, reversible enhancement effects caused by humidity-induced trap state passivation. Together, the AsG-KWW model offers a comprehensive representation of QDs' light intensity evolution under coupled temperature-humidity stress, aligning well with the underlying degradation and recovery mechanisms observed experimentally.

In Eq. (3), seven parameters must be determined for each aging curve. To enhance both fitting efficiency and accuracy, GA was employed. Table II summarized the optimized fitting parameters for each sample under the tested temperature-humidity conditions and the corresponding fitting curves are presented in Fig. 5. The AsG-KWW model demonstrates excellent agreement with the experimental data across various aging environments. In Fig. 5a, b, d, e and f, the fitting curves almost completely overlap or closely follow measure data, indicating that the model effectively captures the temporal evolution of light intensity. In Fig. 5c, although the fitting curve generally follows the overall trend of the experimental data, local deviations are observed, which may be attributed to data fluctuations. Utilizing the predictive capability of the AsG-KWW model, the aging process was extrapolated to

Table II
Fitting parameters by GA for experimental curves. Fval is the optimum value of fitness function.

Condition	τ (h)	β	C	t_0 (h)	σ_1 (h)	σ_2 (h)	α	fval
40 °C, 80% RH	116,806.730	0.285	0.155	771.314	477.211	302.082	6.000	0.013
	193,592.664	0.253	0.163	603.160	347.729	447.295	6.000	0.014
	134,390.191	0.243	0.193	653.521	438.198	472.031	6.000	0.011
	174,295.113	0.245	0.164	500.529	320.187	498.662	6.000	0.011
	195,095.194	0.254	0.160	617.805	383.566	381.696	6.000	0.009
	190,242.837	0.234	0.204	655.993	407.378	451.096	6.000	0.011
60 °C, 60% RH	114,763.600	0.125	0.395	301.994	191.107	269.554	6.000	0.004
	78,058.595	0.126	0.423	272.877	154.619	354.601	6.000	0.003
	85,996.802	0.128	0.412	330.936	203.713	342.644	6.000	0.005
	50,220.012	0.145	0.408	459.473	317.408	187.021	6.000	0.005
	100,641.913	0.136	0.369	492.051	356.360	97.977	6.000	0.005
	101,197.409	0.105	0.483	428.545	296.860	190.631	6.000	0.007
60 °C, 70% RH	138,073.152	0.081	0.593	501.570	342.834	496.193	6.000	0.022
	63,842.910	0.063	0.677	416.758	304.249	463.623	6.000	0.023
	129,850.855	0.073	0.582	448.850	319.850	456.163	6.000	0.020
	85,036.204	0.052	0.849	420.358	319.030	499.887	6.000	0.022
	110,337.617	0.083	0.592	412.127	285.359	494.363	6.000	0.016
	47,941.851	0.116	0.498	320.535	216.634	499.991	6.000	0.023
60 °C, 80% RH	2825.425	0.341	0.200	284.037	161.982	63.301	4.000	0.018
	825.351	0.397	0.489	299.933	185.331	42.424	4.000	0.013
	776.466	0.321	0.637	283.071	191.504	55.097	4.000	0.013
	1460.948	0.192	0.681	262.293	192.842	72.044	4.000	0.026
	2521.408	0.284	0.361	252.340	146.440	82.565	4.000	0.015
	2252.828	0.264	0.405	289.440	179.633	51.266	4.000	0.010
60 °C, 90% RH	9190.182	0.257	0.396	216.622	83.608	53.924	2.000	0.015
	15,154.922	0.283	0.267	203.537	59.127	144.398	2.000	0.021
	15,962.474	0.207	0.348	184.013	51.612	273.577	2.000	0.014
	18,395.883	0.356	0.167	212.168	82.795	48.718	2.000	0.008
	8919.569	0.263	0.349	222.456	101.631	32.546	2.000	0.012
	22,359.940	0.228	0.216	185.531	51.424	79.727	2.000	0.015
80°C, 80% RH	362.799	0.165	0.158	50.243	18.371	130.348	2.000	0.007
	581.339	0.179	0.221	57.292	19.950	44.513	2.000	0.013
	989.942	0.219	0.243	90.410	22.607	279.688	2.000	0.014
	1761.093	0.238	0.178	57.689	10.012	120.685	2.000	0.008
	696.001	0.206	0.267	105.880	36.185	119.859	2.000	0.012
	1599.290	0.157	0.268	115.254	32.820	114.581	2.000	0.013

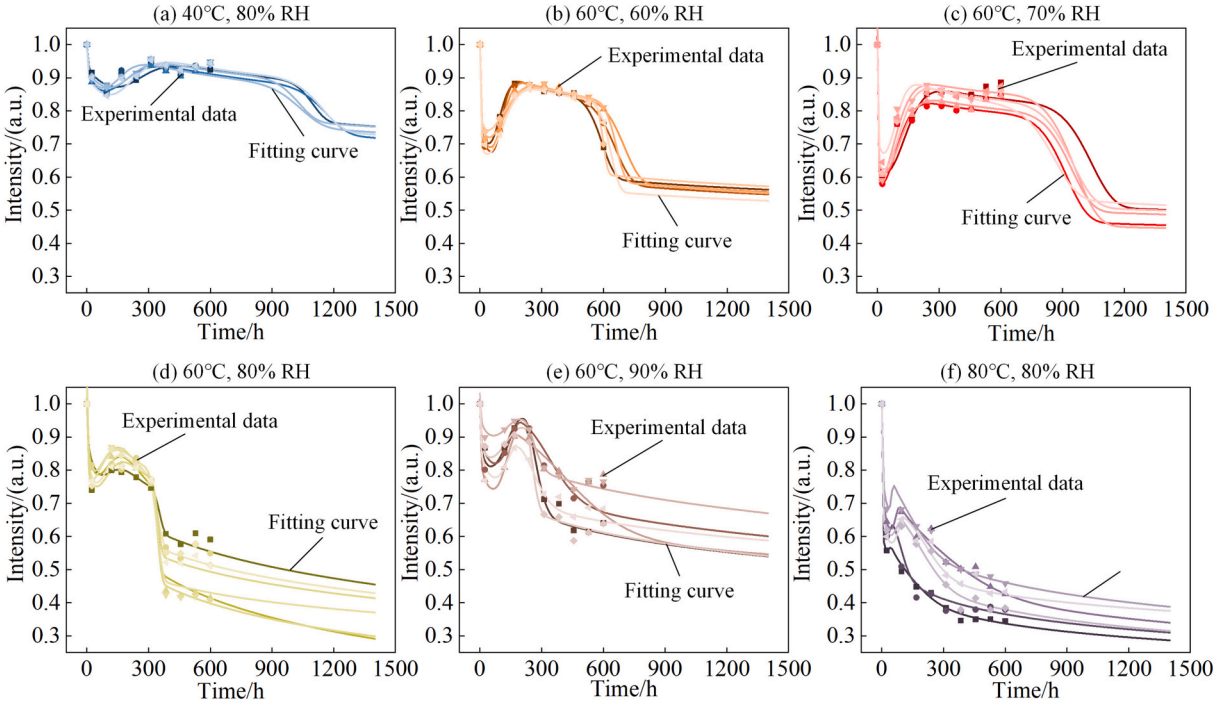

Fig. 5. Fitting curves by AsG-KWW model. (a) 40 °C, 80% RH, (b) 60 °C, 60% RH, (c) 60 °C, 70% RH, (d) 60 °C, 80% RH, (e) 60 °C, 90% RH, and (f) 80 °C, 80% RH.

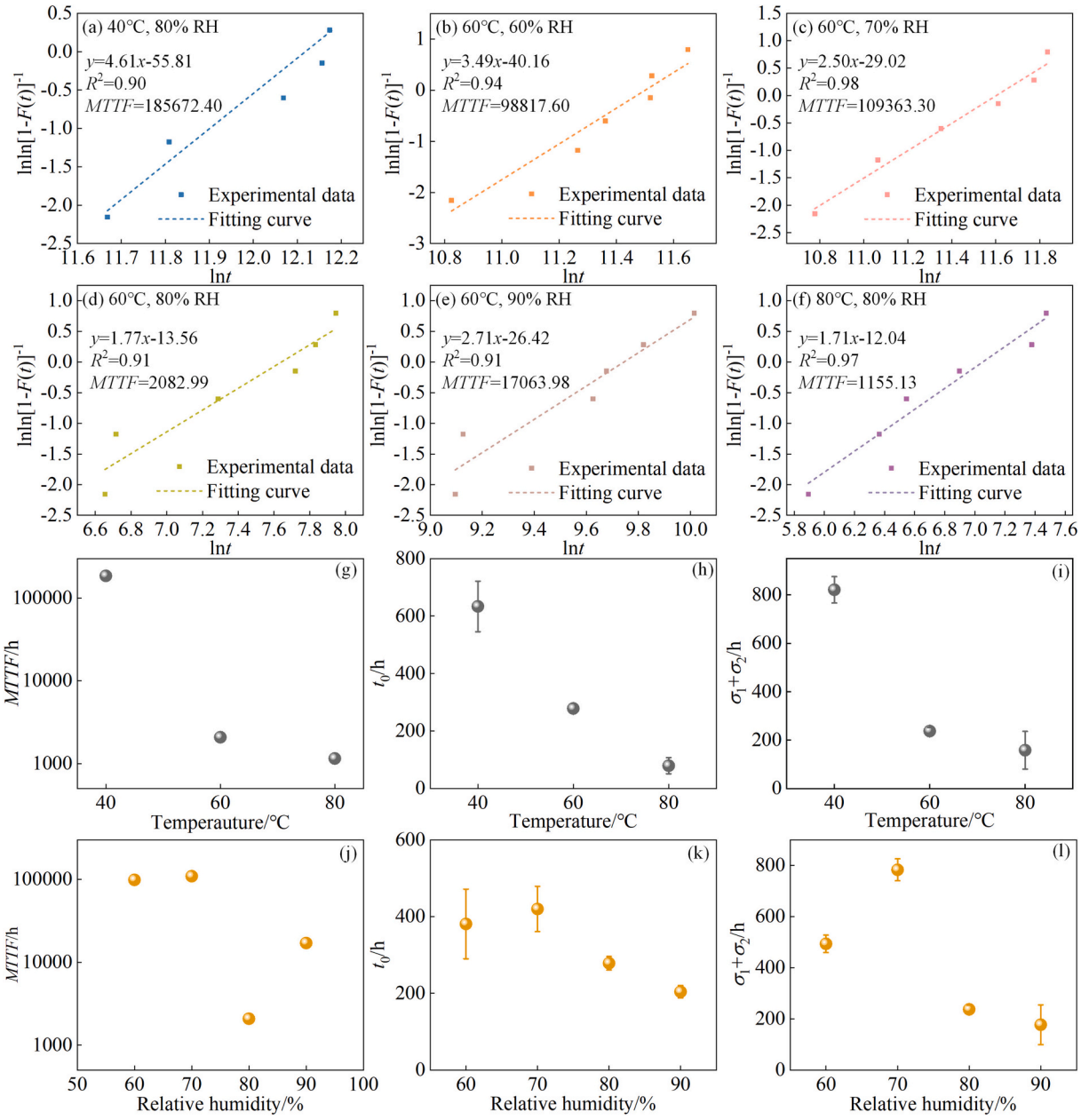

Fig. 6. Parameters comparison. Weibull distribution fitting of MTTF under (a) 40 °C, 80% RH, (b) 60 °C, 60% RH, (c) 60 °C, 70% RH, (d) 60 °C, 80% RH, (e) 60 °C, 90% RH, and (f) 80 °C, 80% RH, (g) MTTF variation with temperature, (h) t_0 variation with temperature, (i) $\sigma_1 + \sigma_2$ variation with temperature (j) MTTF variation with humidity, (k) t_0 variation with humidity, (l) $\sigma_1 + \sigma_2$ variation with humidity.

1500 h. The extended curves reveal a consistent aging pattern composed of three distinct stages: 1) Sharp initial drop; 2) Recovery; 3) Stable attenuation. Due to limitations of in the experimental testing duration and data sampling intervals, some stages may not be fully captured in the raw measurements. The extended fitting curves provide a more complete view of the degradation process and offer valuable insights into the long-term behavior of QDs composites under coupled temperature-humidity stress. In Fig. 5a-f, all three aging stages are clearly revealed in the extended curves generated by the AsG-KWW model. Among them, the aging curve under T40H80 condition exhibits the longest recovery stage, with a relatively slow overall intensity decline throughout the aging period. In contrast, the fitting curve under T80H80 condition (Fig. 5f) indicates the presence of a weak recovery stage, which is difficult to discern from the experimental data. By employing the AsG-KWW model, the underlying details of the aging process can be visualized and analyzed more comprehensively. This allows for a deeper understanding of how different temperature-humidity combinations influence the light intensity evolution of QDs composites.

The characteristic lifetime of QDs composite is a critical parameter for evaluating device performance and reliability. Fig. 6 presents the Weibull distribution fitting results for the six sets of aging conditions. All the samples exhibit a high value of goodness of fit ($R^2 > 0.9$), confirming that the MTTF distribution of QDs composites under temperature-humidity stress conforms well to the Weibull distribution model. The MTTF values calculated using Eq. (10) are as follows: 185672.40 h for T40H80, 98817.60 h for T60H60, 109363.30 h for T60H70, 2082.99 h for T60H80, 17063.98 h for T60H90, and 1155.13 h for T80H80. Fig. 6g

and j illustrate the variation of MTTF with temperature and humidity, respectively. As temperature increased, MTTF declined sharply, with a decreasing rate that slowed at higher temperatures, which highlighted the dominant role of thermal stress in accelerating degradation. In contrast, the influence of humidity on MTTF is less consistent. While MTTF generally decreased with rising humidity, there were irregularities at 70% and 90% RH, possibly due to competing mechanisms of humidity-induced passivation and degradation. Overall, MTTF is more sensitive to temperature than humidity. The turning point of intensity from rising to falling is denoted as t_0. Fig. 6h and k show how t_0 varied with temperature and humidity. As temperature increased, t_0 significantly decreased, from 633 h under T40H80 to 79 h under T80H80. Under increasing humidity, t_0 initially rose from 380 h at T60H60 to 420 h at T60H70, then dropped to 204 h at T60H90. This again suggests that temperature exerts a strong influence than humidity within the testing range. The value of $\sigma_1 + \sigma_2$ derived from AsG-KWW model, represents the duration of the recovery stage. Its variation with temperature and humidity closely followed the trend of t_0. Smaller value of t_0 and $\sigma_1 + \sigma_2$ indicate a shortened of intensity rise duration and recovery stage. Notably, the aging curve under T80H80 closely followed the base line KWW model, with only a minimal recovery effect. Similar behavior was observed in Xie's study, where the aging curve of QDs under 85 °C and 85% RH exhibited an exponential decay. [19] At high temperature and humidity, the diminishing recovery stage implies a weakening of humidity-induced intensity enhancement. In such cases, degradation driven by the coupled effects of thermal and humidity stress dominates the aging process. These findings collectively indicate that the recovery phenomenon primarily occurs under relatively mild aging conditions, and that temperature plays a more significant role than humidity in determining the aging behavior and operational lifetime of QDs composites.

4. Conclusion

In this work, the aging performance of QDs composites under coupled temperature-humidity stress was systematically investigated. The samples exhibited complex intensity evolution behavior, characterized by both rise and decline process within a single aging curve. For example, at T60H80, intensity firstly dropped by about 20% at 24 h, then increased to around 85% at 240 h, and it dropped to around 50% at 384 h once again. By analyzing the underlying mechanisms of intensity enhancement and degradation, an AsG-KWW model was developed, which demonstrated excellent agreement with the experimental data across various aging conditions. Based on the model fitting results, three typical stages were identified to describe the aging behavior of QDs under temperature-humidity dual stress: 1) sharp initial drop, 2) recovery, and 3) stable attenuation. The AsG-KWW model enabled extraction of MTTF for each condition, revealing a dramatic decline in lifetime under high-temperature and high-humidity environments. At 80%RH, the MTTF declined from 98,817.60 h to 1155.13 h when temperature increased from 40 °C to 80 °C. At 60 °C, it generally decreased from 98,817.60 h to 17,063.98 h when humidity increased from 60%RH to 90%RH. Notably, the recovery stage was found to exist only under relatively mild aging conditions, and its presence and duration were significantly influenced by both temperature and humidity, with temperature exerting a more dominant effect. The value of $\sigma_1 + \sigma_2$ decreased from 821.18 h to 158.26 h as temperature increased from 40 °C to 80 °C at 60%RH, while that decreased from 493.75 h to 177.18 h from 60%RH to 90%RH at 60 °C.

CRediT authorship contribution statement

Xuan Yang: Conceptualization, Methodology, Software, Writing – original draft, Writing – review & editing. **Linyi Xiang:** Data curation, Investigation, Formal analysis, Validation. **Bin Xie:** Supervision, Project administration, Writing – review & editing. **Xiaobing Luo:** Supervision, Funding acquisition, Writing – review & editing.

Declaration of competing interest

The authors declare that they have no known competing financial interests or personal relationships that could have appeared to influence the work reported in this paper.

Acknowledgements

This work is supported by the National Natural Science Foundation of China (52106089), and the Natural Science Foundation of Hubei Province (2024AFB618).

Data availability

Data will be made available on request.

References

[1] Z. Wang, M. Liang, Y. Wang, H. Wang, L. Wang, L. Zhao, S. Li, Y. Liu, Optimization of the hole-injection layer for quantum dot light-emitting diodes, Nanoscale 17 (22) (2025) 13581–13593.
[2] S. Ghanbarlou, D. Kahforoushan, H. Abdollahi, P. Zarrintaj, A. Alomar, C. Villanueva, S.M. Davachi, Advances in quantum dot-based fluorescence sensors for environmental and biomedical detection, Talanta 294 (2025) 128176.
[3] A. Sharma, D. Yoo, H.-N. Kim, M.-J. Choi, Sequential surface tailoring from colloid to solid in Ag2Te colloidal quantum dots enables high hole mobility and efficient shortwave infrared photodetection, Nano Energy 141 (2025) 111091.
[4] D. Zhu, S. Jiang, Y. Wang, D. Liu, W. Bao, L. Liu, J. Qu, Y. Wang, C. Liao, Three-dimensional direct lithography of stable quantum dots in hybrid glass, Int. J. Extreme Manuf. 7 (3) (2025) 035503.
[5] H. Choi, D. Shin, W.K. Bae, H. Lee, Enhanced stability of Cd-free quantum dot light-emitting diodes via yttrium acetate-modified ZnMgO: suppressing Mg migration, Adv. Opt. Mater. (2025) 2500988.
[6] H. Moon, C. Lee, W. Lee, J. Kim, H. Chae, Stability of quantum dots, quantum dot films, and quantum dot light-emitting diodes for display applications, Adv. Mater. 31 (34) (2019) 1804294.
[7] Y. Zhao, C. Riemersma, F. Pietra, R. Koole, C. Donega, A. Meijerink, High-temperature luminescence quenching of colloidal quantum dots, ACS Nano 6 (10) (2012) 9058–9067.
[8] S. Huang, Z. Li, B. Wang, N. Zhu, C. Zhang, L. Kong, Q. Zhang, A. Shan, L. Li, Morphology evolution and degradation of $CsPbBr_3$ nanocrystals under blue light-emitting diode illumination, ACS Appl. Mater. Interfaces 9 (8) (2017) 7249–7258.
[9] H. Liu, G. Jin, J. Wang, W. Zhang, L. Qing, Y. Zhang, Q. Lu, P. Yue, G. Zhang, J. Wei, H. Li, H.-L. Wang, Quantum dots mediated crystallization enhancement in two-step processed perovskite solar cells, Nano Micro Lett. 17 (1) (2025) 169.
[10] X. Yang, B. Xie, X. Luo, Resisting oxygen/moisture permeation in quantum dots converted optoelectronic devices, J. Phys. D. Appl. Phys. 57 (48) (2024) 483001.
[11] C. Zhong, K. Yu, Y. Qie, Y. Yu, Y. Lu, G. Deng, T. Guo, H. Hu, F. Li, Ultrahigh-resolution full-color quantum dot LEDs based on region-selective interfacial self-assembly, Adv. Funct. Mater. 35 (47) (2025) 2510076.
[12] Q. Nie, J. Fan, R. Xu, Z. Yao, Y. Xiao, C. Xiang, L. Qian, T. Zhang, Direct optical patterning of quantum dot light-emitting diodes based on ultrafast, low-energy, site-controlled click chemistry reaction, Adv. Funct. Mater. 35 (29) (2025) 2420829.
[13] J. Li, X. Ding, Y. Shi, J. Li, Z. Deng, J. Qiu, J. Zhang, W. Luo, G. Liang, L. Zhao, Y. Tang, A.Q. Liu, Z. Li, Bioinspired ultrathin photonic color convertors for highly efficient micro-light-emitting diodes, FlexMat 1 (3) (2024) 258–268.
[14] S. Zhou, B. Xie, X. Yang, X. Zhang, X. Luo, Superior hydrophobic silica-coated quantum dot for stable optical performance in humid environments, Nanotechnology 33 (19) (2022) 195202.
[15] S. Zou, Y. Liu, J. Li, C. Liu, R. Feng, F. Jiang, Y. Li, J. Song, H. Zeng, M. Hong, X. Chen, Stabilizing cesium lead halide perovskite lattice through Mn(II) substitution for air-stable light-emitting diodes, J. Am. Chem. Soc. 139 (33) (2017) 11443–11450.
[16] R. Liu, F. Fang, P. Liu, X. Duan, K. Wang, X.W. Sun, Liquid-encapsulated quantum dot for enhanced UV and thermal stability of quantum dot color conversion films, Nano Res. 17 (11) (2024) 10127–10133.
[17] X. Yang, S. Zhou, X. Zhang, L. Xiang, B. Xie, X. Luo, Enhancing oxygen/moisture resistance of quantum dots by short-chain, densely cross-linked silica glass network, Nanotechnology 33 (46) (2022) 465202.
[18] N. Pei, X. Yu, S. Zhou, R. Hu, X. Luo, Experimental investigation on the moisture stability of QDs-LEDs with layered packaging structure, IEEE Photon. Technol. Lett. 32 (22) (2020) 1423–1426.
[19] B. Xie, Y. Cheng, J. Hao, X. Yu, W. Shu, K. Wang, X. Luo, White light-emitting diodes with enhanced efficiency and thermal stability optimized by quantum dots-silica nanoparticles, IEEE T. Electron. Dev. 65 (2) (2018) 605–609.
[20] N. Rabiei, S.H. Amirshahi, M. Haghighat Kish, Description of physical aging kinetics of glassy polymers by interpretation of parameters of the Kohlrausch-

Williams-Watts relaxation function via simulation, Phys. Rev. E 99 (3) (2019) 032502.
[21] J. You, J. Lu, Y. Zhu, Q. Yang, J. Zhu, J. Huang, Y. Sun, Identification of multimodel LPV models with asymmetric Gaussian weighting, J. Appl. Math. 2013 (1) (2013) 840628.
[22] E.Y. Wu, R.P. Vollertsen, On the weibull shape factor of intrinsic breakdown of dielectric films and its accurate experimental determination-part I: theory, methodology, experimental techniques, IEEE T. Electron. Dev. 49 (12) (2002) 2131–2140.
[23] W.B. Nelson, Accelerated Testing: Statistical Models, Test Plans, and Data Analysis, John Wiley & Sons, USA, 2009.